Impact-picture phenomenology for $\pi^{\pm}p$, $K^{\pm}p$ and pp, $\bar{p}p$ elastic scattering at high energies

C. Bourrely[1], J. Soffer[1], T.T. Wu[2,3]

[1] Centre de Physique Théorique[a], CNRS-Luminy Case 907, 13288 Marseille Cedex 9, France
[2] Gordon McKay Laboratory, Harvard University Cambridge, MA 02138, USA
[3] Theoretical Physics Division, CERN, 1211 Geneva 23, Switzerland

Abstract. We present an extension to $\pi^{\pm}p$ and $K^{\pm}p$ elastic scattering at high energies of the impact-picture phenomenology we first proposed more than twenty years ago, for pp and $\bar{p}p$ elastic scattering. We show, in particular, that the analytic form of the opacity function for the proton obtained previously is compatible with the experimental results on πp and Kp elastic scattering at high energies. It is proposed that $\pi^{\pm}$ and $K^{\pm}$ external beams be provided from CERN-LHC, so that their elastic scattering from protons can be studied at higher energies. Our phenomenology for pp and $\bar{p}p$ elastic scattering is updated by including new data and we give predictions for future experiments at BNL-RHIC and CERN-LHC.

1 Introduction

In 1967, the Atomic Energy Commission, the predecessor to the present Department of Energy, announced the project to construct a 200 GeV proton accelerator at the Fermi National Accelerator Laboratory. This accelerator makes it possible to study the interaction between two protons both highly relativistic in the center-of-mass system. This announcement motivated Cheng and one of the authors to initiate a program, using relativistic gauge quantum field theory, to study the high-energy behavior of hadron scattering. Perhaps the most unexpected result from this study is that all total cross sections must increase without bound at high energies [1–3]. Another motivation for that investigation was to accept the challenge issued by Oppenheimer [4] at his concluding talk at the 1958 Rochester meeting at CERN. He said at that time: "There are areas where we know very little – extremely high-energy collisions, for example – where little can be done by anyone."

Three years after the theoretical prediction of the increasing total cross sections, experiments at the CERN Intersecting Storage Rings confirmed that the proton-proton total cross section indeed turned around and started to increase [5,6], and these data made possible to give the first quantitative predictions for future experiments on the total cross sections for $p\bar{p}, \pi^{\pm}p, K^{\pm}p$ [7]. Careful phenomenology incorporating these increasing hadronic cross sections, called the impact picture, was first carried out in 1978 [8]. Five years later, when more data became available, the parameters of this phenomenology were revised

[9]. It was found that the changes of the values are quite small. These revised parameters have been used extensively to make various predictions, including for example the Coulomb interference effects and increasing integrated elastic cross section for proton–proton scattering up to 40 TeV in the center-of-mass energy, the proposed energy for the Superconducting Super Collider which was never built [10]. All the predictions that can be confirmed experimentally have been confirmed [11]. A recent chapter in a book gives a summary of the development up to this point [3]. Nevertheless, since it is by now nearly two decades since the 1984 parameters were obtained, it is the opportune time to take another look at the parameters. This is one of the purposes of the present paper. Another purpose is to extend the phenomenology from the cases of proton–proton and proton–antiproton scattering to four other processes, namely $\pi^{\pm}p, K^{\pm}p$. The increasing total cross sections for these four processes were last investigated in 1973, nearly thirty years ago, and these predictions are in an even greater need of updating. It should perhaps be mentioned that the 1973 prediction for the $\pi^{-}p$ case has been well confirmed by later data [12].

When we made our previous analysis in 1979 and 1984, some experimental data were still preliminary, but since then they have been completed, so it is worth to "revisit" our model by making an analysis with a full set of final data points. In the next section, we recall the main features of the model we use to describe elastic scattering and we will explain our parametrization. Section 3 is devoted to the presentation of the numerical results for πp, Kp scattering and for pp, $\bar{p}p$ scattering with some comparison between the present and the previous determination of

---

[a] Unité Propre de Recherche 7061

the parameters. We also give predictions for future experiments at BNL-RHIC and CERN-LHC. Our concluding remarks are given in Sect. 4.

2 Description of the scattering amplitudes

In the impact-picture representation, the spin-independent scattering amplitude[1], for pp and $\bar{p}p$ elastic scattering, reads

$$a(s,t) = \frac{\mathrm{i}s}{2\pi} \int e^{-\mathrm{i}\boldsymbol{q}\cdot\boldsymbol{b}}(1 - e^{-\Omega_0(s,\boldsymbol{b})})\mathrm{d}\boldsymbol{b}, \qquad (1)$$

where $\mathbf{q}$ is the momentum transfer ($t = -\mathbf{q}^2$) and $\Omega_0(s,\boldsymbol{b})$ is defined to be the opaqueness at impact parameter $\mathbf{b}$ and at a given energy s. We take

$$\Omega_0(s,\boldsymbol{b}) = S_0(s)F(\boldsymbol{b}^2) + R_0(s,\boldsymbol{b}); \qquad (2)$$

the first term is associated with the "pomeron" exchange, which generates the diffractive component of the scattering and the second term is the Regge background. The pomeron energy dependence is given by the crossing symmetric expression [1,2]

$$S_0(s) = \frac{s^c}{(\ln s)^{c'}} + \frac{u^c}{(\ln u)^{c'}}, \qquad (3)$$

where u is the third Mandelstam variable. The choice one makes for $F(\boldsymbol{b}^2)$ is crucial and we take the Bessel transform of

$$\tilde{F}(t) = f[G(t)]^2 \frac{a^2 + t}{a^2 - t}, \qquad (4)$$

where $G(t)$ stands for the proton "nuclear form factor", parametrized like the electromagnetic form factor, as having two poles,

$$G(t) = \frac{1}{(1 - t/m_1^2)(1 - t/m_2^2)}. \qquad (5)$$

The slowly varying function occurring in (4) reflects the approximate proportionality between the charge density and the hadronic matter distribution inside a proton. So the pomeron part of the amplitude depends on only *six* parameters c, c', m_1, m_2, f, and a. The asymptotic energy regime of hadronic interactions are controlled by c and c', which will be kept, for all elastic reactions, at the values obtained in 1984 [9], namely

$$c = 0.167 \quad \text{and} \quad c' = 0.748. \qquad (6)$$

The remaining four parameters are related more specifically to the reaction pp ($\bar{p}p$) and they will be slightly re-adjusted from the use of a new set of data.

---

[1] Here we neglect the spin-dependent amplitude which was considered in [8,13] for the description of polarizations and spin correlation parameters

We now turn to the Regge background. A generic Regge exchange amplitude has an expression of the form

$$\tilde{R}_i(s,t) = C_i e^{b_i t} \left[1 \pm e^{-\mathrm{i}\pi\alpha_i(t)} \right] \left(\frac{s}{s_0} \right)^{\alpha_i(t)}, \qquad (7)$$

where $C_i e^{b_i t}$ is the Regge residue, $\pm$ is the signature factor, $\alpha_i(t) = \alpha_{0i} + \alpha_i' t$ is a standard linear Regge trajectory and $s_0 = 1\,\text{GeV}^2$. If we consider the sum over all the allowed Regge trajectories, $\tilde{R}_0(s,t) = \sum_i \tilde{R}_i(s,t)$, the Regge background $R_0(s,\boldsymbol{b})$ in (2) is the Bessel transform of $\tilde{R}_0(s,t)$. In pp ($\bar{p}p$) elastic scattering, the allowed Regge exchanges are A_2, ρ, ω, so the Regge background involves several additional parameters; we will come back to them.

For completeness, in order to describe the very small t region, one should add to the hadronic amplitude considered above the Coulomb amplitude whose expression is $a^C(s,t) = 2\alpha[s/|t|]G_{\text{em}}^2(t)\exp[\pm\mathrm{i}\alpha\phi(t)]$, where α is the fine structure constant, $G_{\text{em}}(t)$ is the electromagnetic form factor, $\phi(t)$ is the West–Yennie phase [14], and the $\pm$ sign corresponds to pp and $\bar{p}p$.

Let us now consider the case of πp elastic scattering. The scattering amplitude is also defined by (1) and we keep the same structure for the opaqueness (2). However, for the pomeron exchange, we assume that the nuclear matter density is the product of the proton and the pion contributions. So with this reasonable hypothesis, we write similarly to (4)

$$\tilde{F}(t) = f_\pi G(t)F_\pi(t)\frac{a_\pi^2 + t}{a_\pi^2 - t}. \qquad (8)$$

Here $G(t)$ is given by (5) with the same parameters values m_1, m_2 as in the proton case and $F_\pi(t)$ is the pion "nuclear form factor", we parametrize like the pion electromagnetic form factor, as a single pole $1/(1 - t/m_{3\pi}^2)$ [15]. Therefore the pomeron term for πp elastic scattering involves *three* additional free parameters f_π, $m_{3\pi}$, and a_π. The Regge background is simpler in this case since the only allowed Regge exchange is ρ and we have taken for the generic amplitude an expression of the form (7), with the same Regge trajectory as before, only the Regge residue being different.

Finally in the case of Kp elastic scattering, for the pomeron exchange the procedure is the same as for πp and the use of an expression like (8) leads to the introduction of *three* further free parameters f_K, m_{3K}, and a_K. However the Regge background is a little bit more complicated, since the allowed Regge exchanges are A_2, ρ, ω, as in the pp ($\bar{p}p$) reaction. The same Regge trajectories will be used and again only the Regge residues are different. Needless to say that the Coulomb amplitude is also included for the πp and Kp cases.

To summarize, for all the cases we are considering, the elastic scattering amplitude reduces to a Bessel transform

$$a(s,t) = \mathrm{i}s \int_0^\infty J_0(b\sqrt{-t})(1 - e^{-\Omega_0(s,\boldsymbol{b})})b\,\mathrm{d}b. \qquad (9)$$

Table 1. Pomeron fitted parameters for pp ($\bar{p}p$). Comparison of the present and 1984 solutions

Year	Present	1984
m_1	0.577	0.586
m_2	1.719	1.704
f	6.971	7.115
a	1.858	1.953

Table 2. pp ($\bar{p}p$) Regge parameters

Exchange	C
A_2	-24.269
ω	-167.329
ρ	124.919

Table 3. Effective Regge trajectories

Trajectory	A_2	ω	ρ
	$0.357 + t$	$0.323 + 0.795t$	$0.320 + t$

Table 4. Detailed χ^2 comparison between the present and 1984 solutions for pp and $\bar{p}p$

Process	χ^2 present	χ^2 1984	nb points
$d\sigma^{pp}/dt\ p_{lab} = 280\,\mathrm{GeV}/c$	351	538	58
$d\sigma^{pp}/dt\ p_{lab} = 496\,\mathrm{GeV}/c$	194	527	54
$d\sigma^{pp}/dt\ p_{lab} = 1061\,\mathrm{GeV}/c$	199	301	62
$d\sigma^{pp}/dt\ p_{lab} = 1486\,\mathrm{GeV}/c$	246	190	16
$d\sigma^{pp}/dt\ p_{lab} = 2060\,\mathrm{GeV}/c$	40	42	10
$d\sigma^{pp}/dt\ p_{lab} = 2080\,\mathrm{GeV}/c$	97	135	51
$d\sigma^{\bar{p}p}/dt\ p_{lab} = 315\,\mathrm{GeV}/c$	51	516	41
$d\sigma^{\bar{p}p}/dt\ \sqrt{s} = 546\,\mathrm{GeV}$	474	1190	84
$d\sigma^{\bar{p}p}/dt\ \sqrt{s} = 630\,\mathrm{GeV}$	141	628	19
σ_{tot}^{pp}	16	144	13
$\sigma_{tot}^{\bar{p}p}$	21	44	10
ρ^{pp}	2	9	7
$\rho^{\bar{p}p}$	8	11	6
Total	1840	4275	431

We define the ratio of real to imaginary parts of the forward amplitude

$$\rho(s) = \frac{\mathrm{Re}\ a(s, t = 0)}{\mathrm{Im}\ a(s, t = 0)}, \qquad (10)$$

the total cross section

$$\sigma_{tot}(s) = \frac{4\pi}{s}\mathrm{Im}\ a(s, t = 0) \qquad (11)$$

and the differential cross section

$$\frac{d\sigma(s, t)}{dt} = \frac{\pi}{s^2}|a(s, t)|^2. \qquad (12)$$

This completes the description of the scattering amplitudes and we now turn to the phenomenological results and predictions for future experiments.

Table 5. Detailed χ^2 for πp fitted processes

Process	χ^2	nb points
$d\sigma(\pi^-p)/dt\ p_{lab} = 100\,\mathrm{GeV}/c$	112	32
$d\sigma(\pi^-p)/dt\ p_{lab} = 200\,\mathrm{GeV}/c$	139	14
$d\sigma(\pi^+p)/dt\ p_{lab} = 100\,\mathrm{GeV}/c$	50	32
$d\sigma(\pi^+p)/dt\ p_{lab} = 200\,\mathrm{GeV}/c$	58	14
$\sigma_{tot}(\pi^-p)$	64	8
$\sigma_{tot}(\pi^+p)$	16	6
$\rho(\pi^-p)$	8	4
$\rho(\pi^+p)$	6	3
Total	453	113

Table 6. Kp Regge parameters

Exchange	C
A_2	6.322
ρ	-39.499
ω	46.539

Table 7. Detailed χ^2 for Kp fitted processes

Process	χ^2	nb points
$d\sigma(K^-p)/dt\ p_{lab} = 100\,\mathrm{GeV}/c$	120	43
$d\sigma(K^-p)/dt\ p_{lab} = 140\,\mathrm{GeV}/c$	16	13
$d\sigma(K^-p)/dt\ p_{lab} = 175\,\mathrm{GeV}/c$	23	15
$d\sigma(K^-p)/dt\ p_{lab} = 200\,\mathrm{GeV}/c$	15	15
$d\sigma(K^+p)/dt\ p_{lab} = 100\,\mathrm{GeV}/c$	56	36
$d\sigma(K^+p)/dt\ p_{lab} = 140\,\mathrm{GeV}/c$	11	16
$d\sigma(K^+p)/dt\ p_{lab} = 175\,\mathrm{GeV}/c$	16	17
$d\sigma(K^+p)/dt\ p_{lab} = 200\,\mathrm{GeV}/c$	17	12
$\sigma_{tot}(K^-p)$	13	17
$\sigma_{tot}(K^+p)$	8	15
$\rho(K^-p)$	16	5
$\rho(K^+p)$	7	8
Total	318	212

3 Phenomenological results and predictions

We have made a global fit for all the elastic reactions under study and for all of them we have introduced a lower cutoff at $p_{lab} = 100\,\mathrm{GeV}/c$. When making the fit we have analyzed high-energy experimental pp ($\bar{p}p$) data including a set of 431 points coming from ISR, SPS and Tevatron experiments on $\rho(s)$, $\sigma_{tot}(s)$ and $d\sigma(s, t)/dt$. The new pp ($\bar{p}p$) pomeron parameters are listed in Table 1 together with those obtained in our previous analysis. We notice that these four parameters have changed only slightly, within a few percents. The C values of the Regge residues are given in Table 2. The parameters b are zero except for the ρ contribution for which we found $b_\rho = 8.54$. Let us notice that the Regge exchanges have been eikonalized so the intercept and the slope of the trajectories are effective parameters whose values are given in Table 3. However we notice that the three intercepts are close to $1/3$ and the A_2 and ρ slopes have the standard value $\alpha' = 1\,\mathrm{GeV}^{-2}$, whereas the ω slope is slightly smaller. A detailed χ^2 anal-
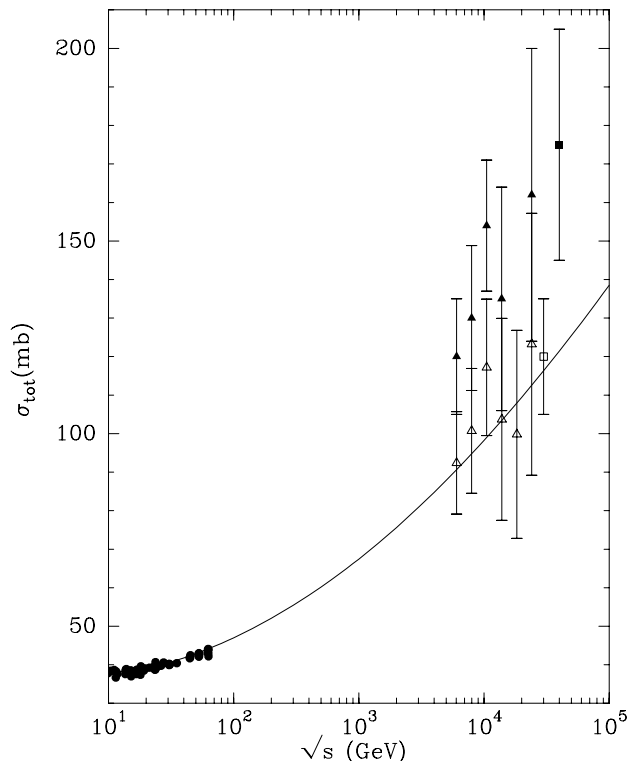
Fig. 1. σ_{tot} for $\bar{p}p$ and pp as a function of $\sqrt{s}$. Data compilation from [16]

Fig. 2. Comparison of σ_{tot} for pp as a function of $\sqrt{s}$ with cosmic ray experiments. Open triangles are from [17] and the open square is from [18]. For the full square and triangles, see the text

ysis is presented in Table 4, where the present solution, which is a fit to the data, is compared to the 1984 solution, which is a prediction made with the same set of data. We notice a substantial improvement in the χ^2, since we have now a $\chi^2/\text{pt} = 4.27$. A comparison of our model with the experimental data is given in Figs. 1–6. In Fig. 2 we extend our prediction to the cosmic ray energy region and our extrapolation of σ_{tot}^{pp} is in agreement with the data points, which have large errors. However, a reanalysis of the same data leads to larger values, as shown in Fig. 2 by the full data points [19,20]. For $\sqrt{s} = 14$ TeV our predicted value is $\sigma_{\text{tot}}^{pp} = 103.5$ mb. In Fig. 5 we note a remarkable description of the $\bar{p}p$ data in the Coulomb interference region. In Figs. 7 and 8, we display some predictions for future measurements at BNL-RHIC [32] and CERN-LHC [33], respectively. It is interesting to note that a dip-bump structure, first observed at ISR energies, is gradually restored as s increases. It moves in around $|t| = 0.5$ GeV^2 at LHC energy with the appearance of another structure around $|t| = 2$ GeV^2.

For $\pi^{\pm}p$ elastic scattering, from 113 data points we have obtained the following pomeron parameters values:

$$m_{3\pi} = 0.766, \quad f_{\pi} = 4.241, \quad a_{\pi} = 2.327.$$

Due to the lack of very high-energy data for these reactions, the Regge contributions play a non-negligible role in the fit we made with a cut at $p_{\text{lab}} = 100$ GeV/c. The only allowed Regge exchange is ρ and we find $C_{\rho} = 4.162$ and $b_{\rho} = 4.270$. A detailed χ^2 analysis of the data is given in Table 5 and we have a $\chi^2/\text{pt} = 4$. A comparison of our

model with the experimental data is given in Figs. 9–12, and in Fig. 13 we give some predictions for future measurements at CERN-LHC. In the TeV energy range we predict the existence of a shoulder between $|t| = 1$ and 2 GeV^2, moving in for increasing energy, and the observation of such pattern will be very important.

Finally for $K^{\pm}p$ elastic scattering where we used 212 data points, the procedure is the same as in the $\pi^{\pm}p$ case and the pomeron parameters obtained from the fit are

$$m_{3K} = 1.139, \quad f_K = 3.673, \quad a_K = 1.991.$$

For these reactions the allowed exchanges are the A_2, ρ and ω. We have kept the same trajectories as in the pp case, with $b_{A2} = b_{\omega} = 8.541$, and $b_{\rho} = 4.270$ and the values of the corresponding C parameters are listed in Table 6. A detailed χ^2 analysis of the data is given in Table 7 and we have a $\chi^2/\text{pt} = 1.5$. A comparison of our model with the experimental data is given in Figs. 14–17, and in Fig. 18 we give some predictions for future measurements at CERN-LHC. It might be possible to expect future measurements at BNL-RHIC with extracted $\pi^{\pm}$, $K^{\pm}$ beams, to improve the available data.
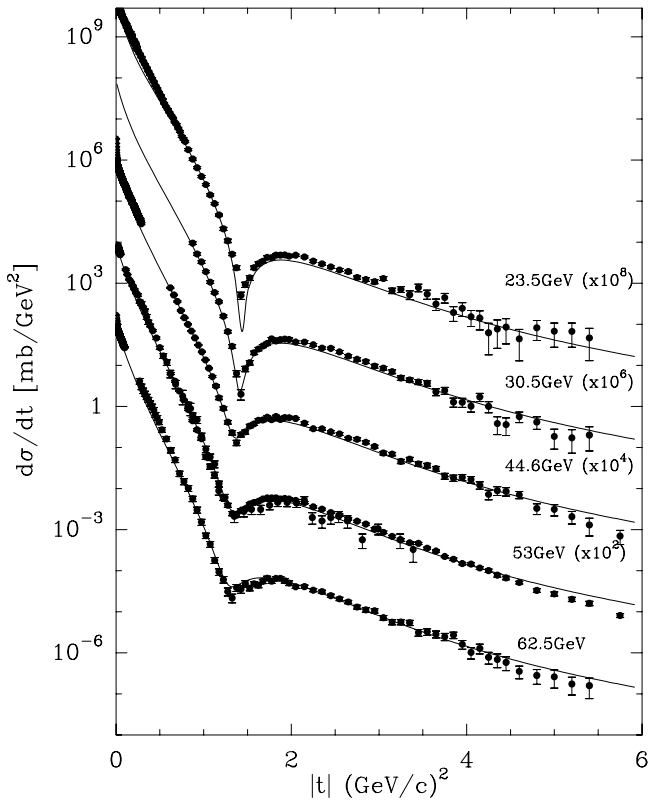
4 Concluding remarks

In one of the earliest phenomenological analyses [7] that incorporated the theoretical predictions of increasing cross
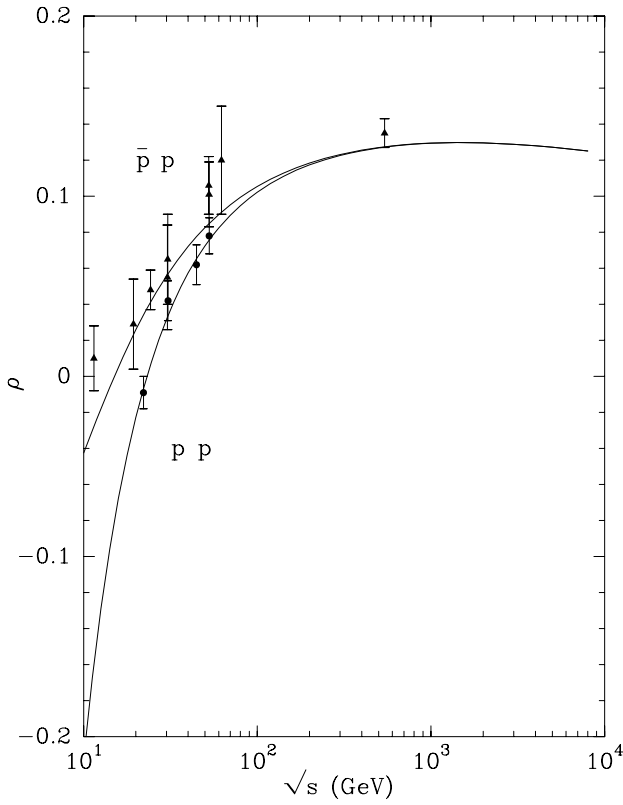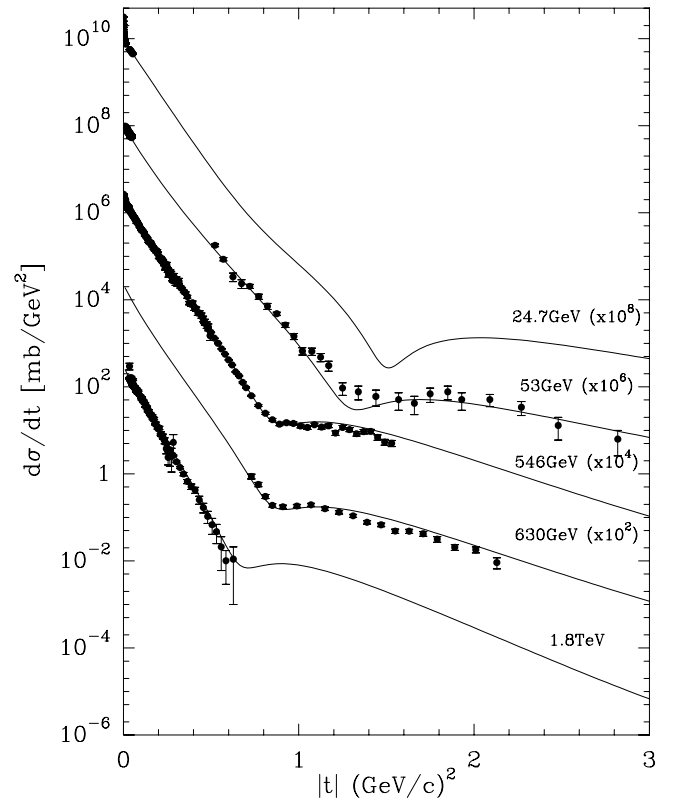
Fig. 3. ρ for pp and $\bar{p}p$ as a function of $\sqrt{s}$. Data compilation from [16] (full triangles $\bar{p}p$ and full circles pp)
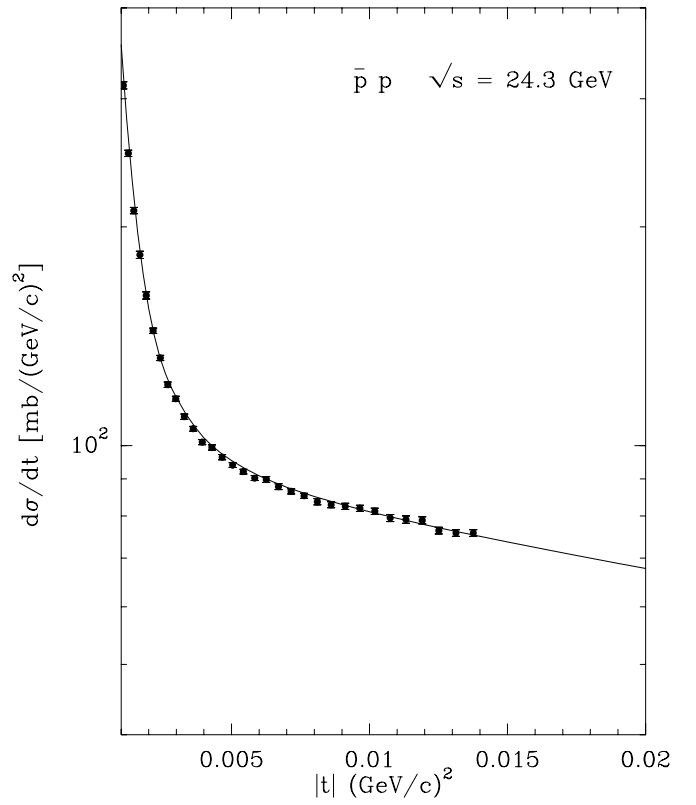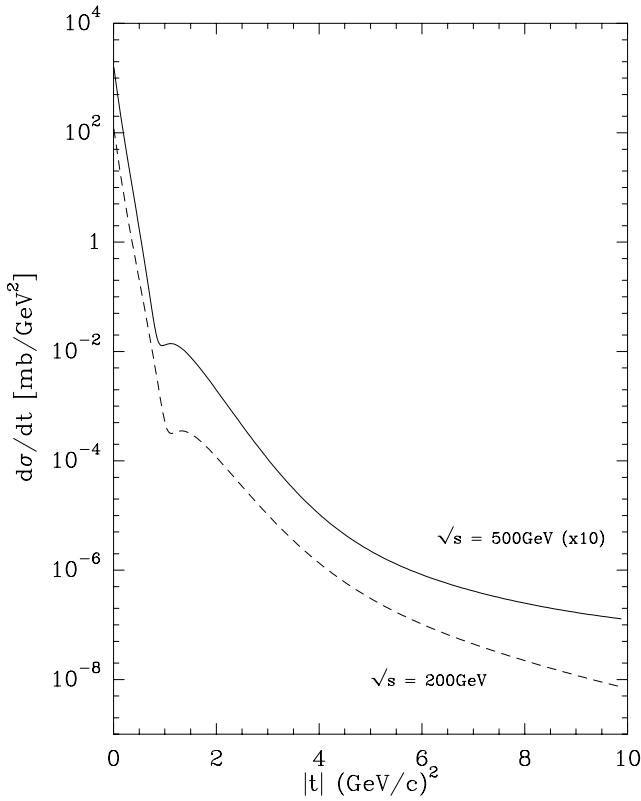

Fig. 5. $d\sigma/dt$ for $\bar{p}p$ as a function of $|t|$ in the small t region for $\sqrt{s} = 24.3$ GeV. Experiment UA6 [27]
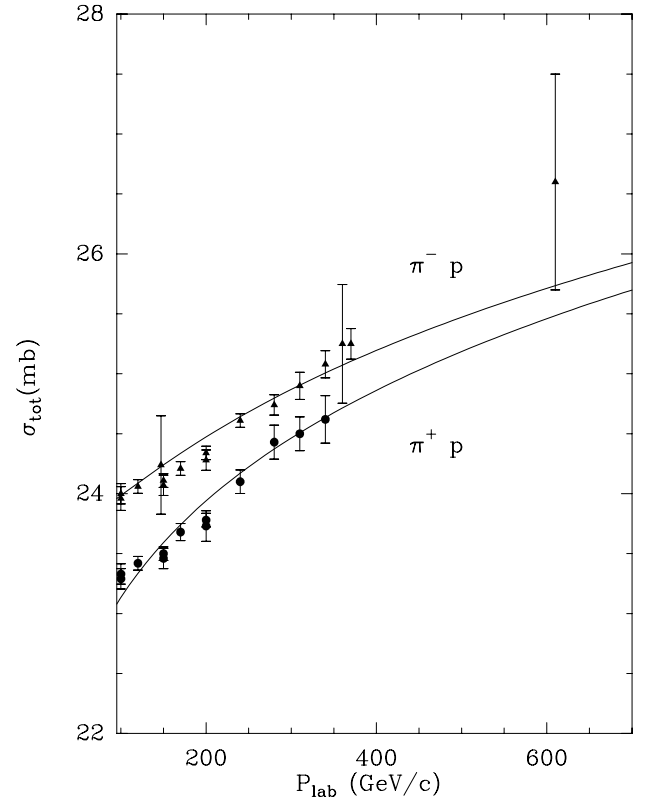

Fig. 4. $d\sigma/dt$ for pp as a function of $|t|$ for $\sqrt{s} = 23.5$, 30.5, 44.8, 53, 62.5 GeV. Experiments from [21–26]
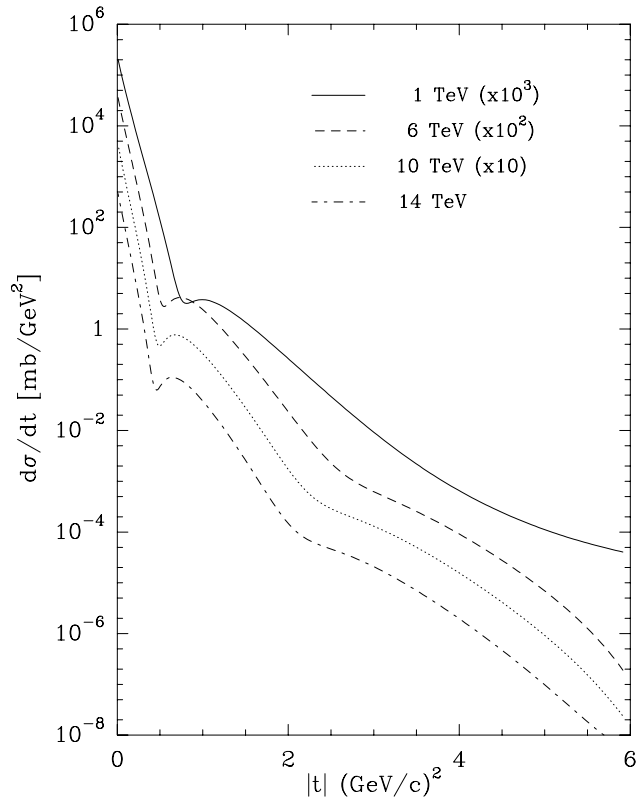

Fig. 6. $d\sigma/dt$ for $\bar{p}p$ as a function of $|t|$ for $\sqrt{s} = 24.7$, 53, 546, 630, 1800 GeV. Experiments from [24, 25, 27–31]

Fig. 7. Predicted $d\sigma/dt$ for pp as a function of $|t|$ for the BNL-RHIC energy domain

Fig. 8. Predicted $d\sigma/dt$ for pp as a function of $|t|$ for different $\sqrt{s}$ in the TeV energy domain

Fig. 9. σ_{tot} for $\pi^{\pm}p$ as a function of p_{lab} (GeV/c). Data compilation from [16]
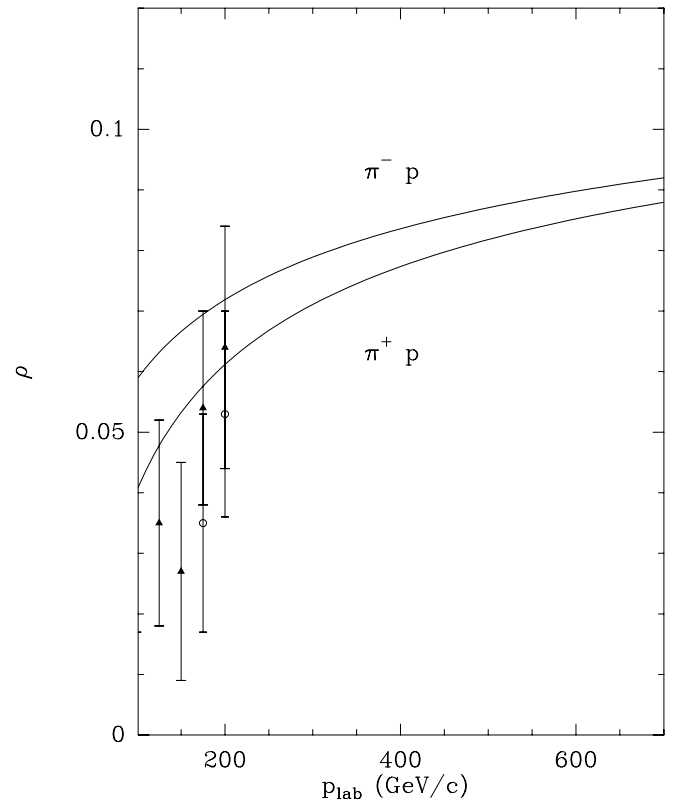
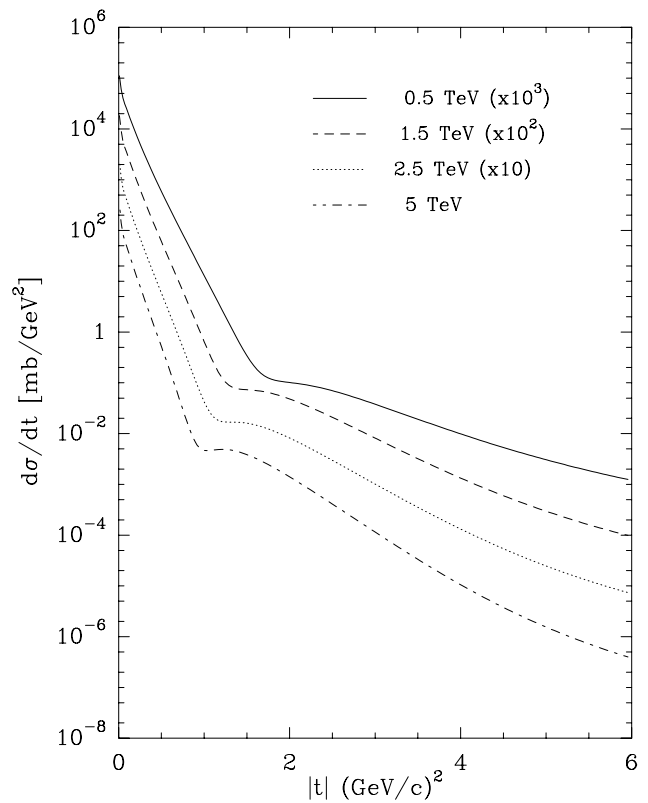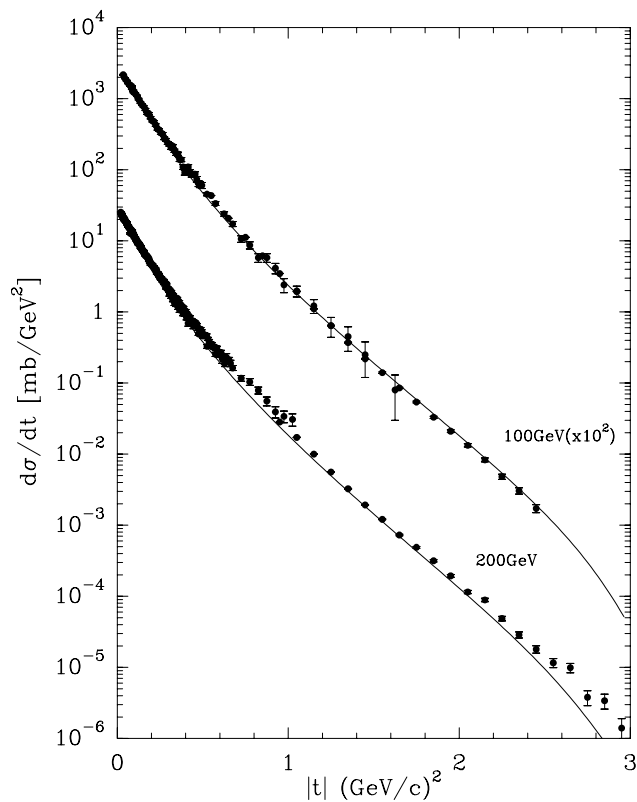

Fig. 10. ρ for $\pi^{\pm}p$ as a function of p_{lab} (GeV/c) (π^- triangles, π^+ open circles). Data compilation from [16]
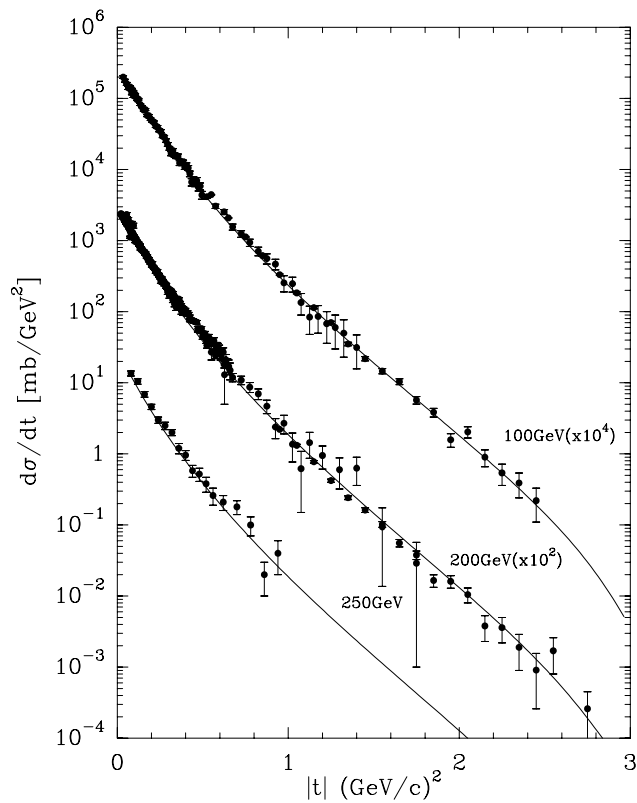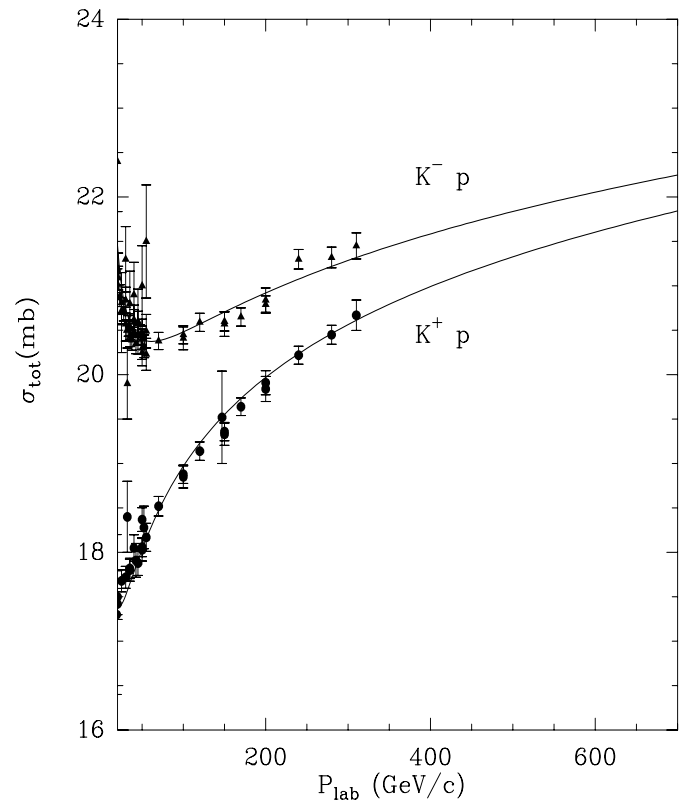
Fig. 11. $d\sigma/dt$ for $\pi^+ p$ as a function of $|t|$ for $p_{\text{lab}} = 100, 200, 250\,\text{GeV}/c$. Experiments from [34–38]

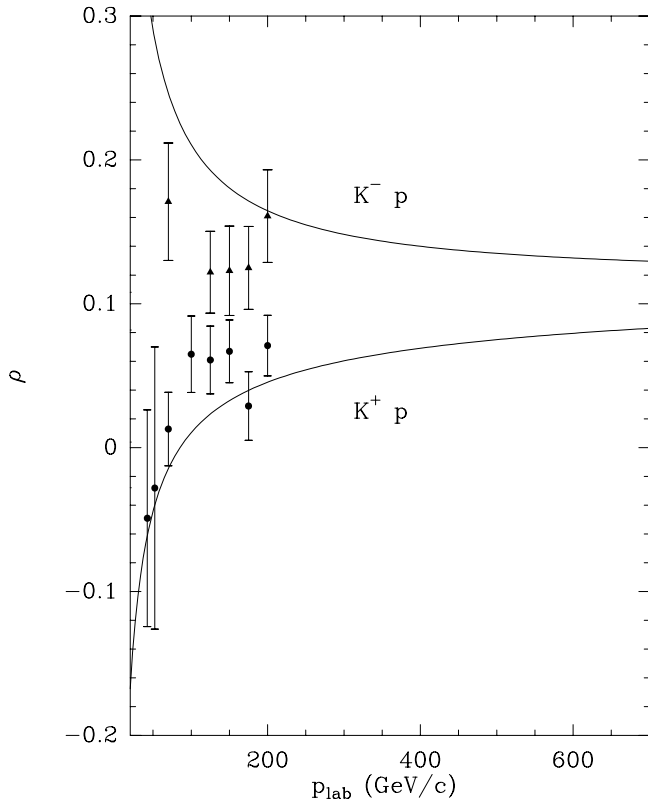

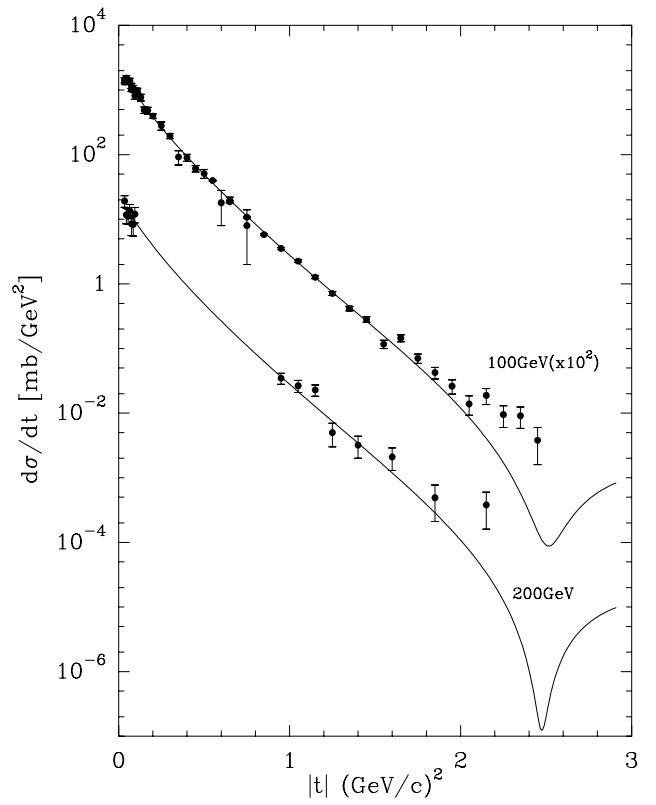**Fig. 13.** $d\sigma/dt$ for $\pi^- p$ as a function of $|t|$ for different $\sqrt{s}$ in the TeV energy domain

Fig. 12. $d\sigma/dt$ for $\pi^- p$ as a function of $|t|$ for $p_{\text{lab}} = 100, 200\,\text{GeV}/c$. Experiments from [34–37]
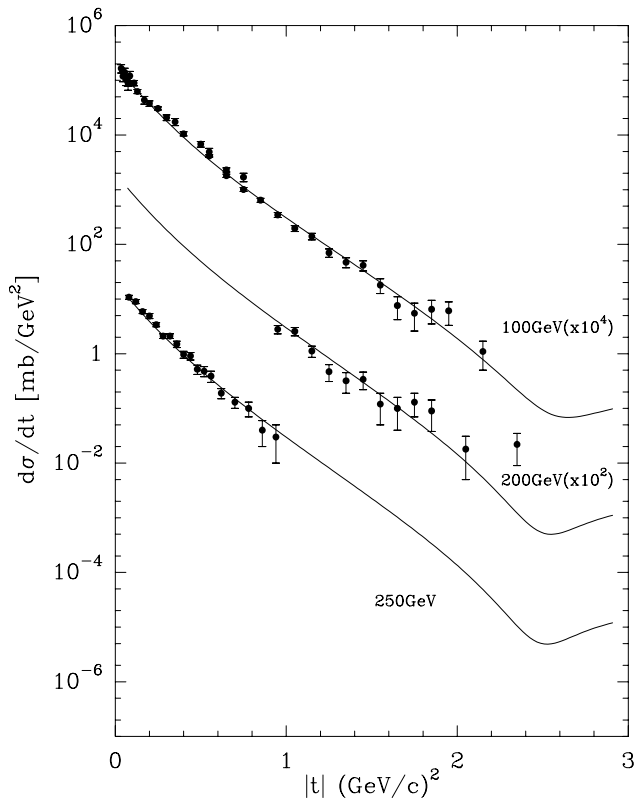

Fig. 14. σ_{tot} for $K^\pm p$ as a function of p_{lab} (GeV/c), compilation of data from [16]
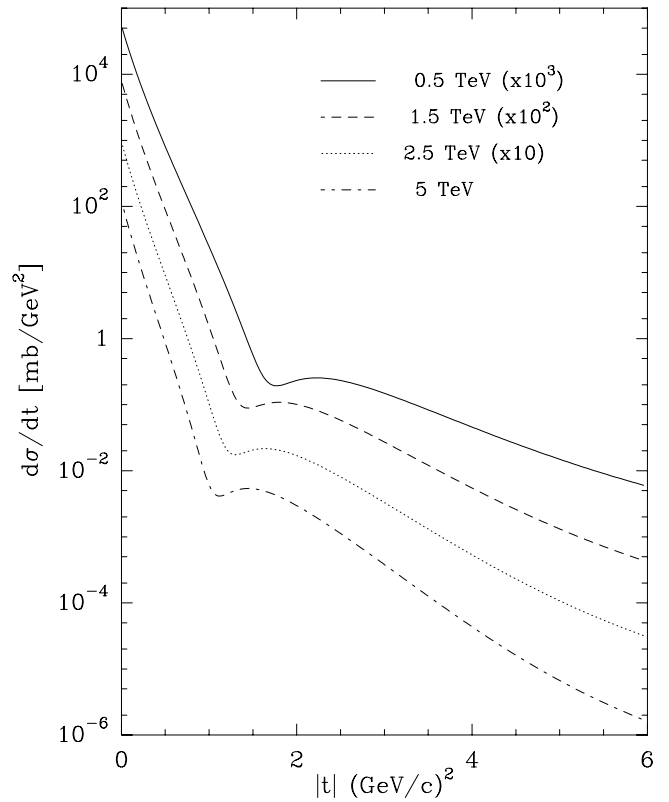
Fig. 15. ρ for $K^\pm p$ as a function of $p_{\text{lab}}(\text{GeV}/c)$, ($K^-$ triangles, K^+ circles). Compilation of data from [16]

Fig. 17. $d\sigma/dt$ for $K^- p$ as a function of $|t|$ for $p_{\text{lab}} = 100$, $200\,\text{GeV}/c$. Experiments from [35, 36, 39]

Fig. 16. $d\sigma/dt$ for $K^+ p$ as a function of $|t|$ for $p_{\text{lab}} = 100$, 200, $250\,\text{GeV}/c$. Experiments from [35, 36, 38, 39]

Fig. 18. $d\sigma/dt$ for $K^- p$ as a function of $|t|$ for different $\sqrt{s}$ in the TeV energy domain

sections [1], results were obtained not only for pp and $\bar{p}p$ total cross sections but also for those of π^+p, π^-p, K^+p and K^-p. Since then, efforts in this direction have been concentrated on studying the cross sections for pp and $\bar{p}p$ scattering [8–11].

There are perhaps two reasons why there has been a lack of progress in the cases of $\pi^\pm p$ and $K^\pm p$ as compared with those of pp and $\bar{p}p$. First, since the available experimental data for $\pi^\pm p$ and $K^\pm p$ scattering are at lower energies, the Regge backgrounds play more prominent roles, and this complicates the phenomenological analysis. Secondly, there has been relatively little reason for analyzing such cases because, while the predictions for the pp and $\bar{p}p$ cases are most relevant with new experimental data expected at higher and higher energies every few years, up until now the availability of high-energy data for $\pi^\pm p$ and $K^\pm p$ elastic scattering has been very limited.

The present work is motivated by the realization that the basis for the second reason may change in the near future. The construction of the CERN-LHC, which is a proton collider of 7 TeV in each beam, will make it possible to have multi-TeV secondary beams of $\pi^\pm$ and $K^\pm$. The scattering of such external secondary beams on protons will provide the much needed data for $\pi^\pm p$ and $K^\pm p$ elastic scattering at high energies (see Figs. 13 and 18). For example, the center-of-mass energy of a 6 TeV $\pi^\pm$ or $K^\pm$ and a stationary proton is about 106 GeV, close to that of ISR for pp scattering. Encouraged by the likely irrelevance of this second reason, it has been possible to overcome the difficulty due to the first reason, namely the inclusion of more elaborate Regge backgrounds.

Looking forward, we believe that the present treatment of $\pi^\pm p$ and $K^\pm p$ elastic scattering will make it possible to deal with a number of additional scattering processes. The most interesting process is perhaps the following:

$$p + p \longrightarrow p + N(1440). \tag{13}$$

This high-energy process was studied nearly thirty years ago [41]. Since $N(1440)$ has the same $I(J^P)$ as the proton, this is one of the simplest diffraction processes. This is to be contrasted with the elastic scatterings dealt with by most of the existing impact-picture phenomenologies, including the present paper. The diffraction process (13) and many similar ones can perhaps be studied experimentally at BNL-RHIC, and we look forward eagerly to such data in the near future.

References

1. H. Cheng, T.T. Wu, Phys. Rev. Lett. **24**, 1456 (1970)
2. H. Cheng, T.T. Wu, Expanding protons: Scattering at high energies (M.I.T. Press, Cambridge, MA 1987)
3. T.T. Wu, Chapter 4.3.4 of Scattering, Scattering and Inverse Scattering in Pure and Applied Science, edited by E.R. Pike, P. Sabatier (Academic Press 2001), p. 1582
4. J.R. Oppenheimer, Concluding Remarks, in Proceedings of the 1958 Annual International Conference on High Energy Physics, CERN, Geneva, Switzerland
5. S.R. Amendolia et al., Phys. Lett. B **44**, 119 (1973)
6. U. Amaldi et al., Phys. Lett. B **44**, 112 (1973)
7. H. Cheng, J.K. Walker, T.T. Wu, Phys. Lett. B **44**, 97 (1973)
8. C. Bourrely, J. Soffer, T.T. Wu, Phys. Rev. D **19**, 3249 (1979)
9. C. Bourrely, J. Soffer, T.T. Wu, Nucl. Phys. B **247**, 15 (1984)
10. C. Bourrely, J. Soffer, T.T. Wu, Z. Physik C **37**, 369 (1988); Erratum-ibid. **53**, 538 (1992)
11. C. Bourrely, J. Soffer, T.T. Wu, Phys. Lett. B **121**, 284 (1983); Phys. Rev. Lett. **54**, 757 (1985); Phys. Lett. B **196**, 237 (1987); Phys. Lett. B **252**, 287 (1990); Modern Phys. Lett. A 6, 72; A **7**, 457 (1991); Phys. Lett. B **315**, 195 (1993); Proceedings of the VIth Blois Workshop, Blois 1995, edited by P. Chiappetta, M. Haguenauer, J. Tran Tanh Van (Editions Frontières 1996), p. 15
12. U. Dersch et al., SELEX Collaboration, Nucl. Phys. B **579**, 277 (2000)
13. C. Bourrely, J. Soffer, T.T. Wu, Phys. Lett. B **76**, 481 (1978); C. Bourrely, H.A. Neal, H.A. Ogren, J. Soffer, T.T. Wu, Phys. Rev. D **26**, 1781 (1982)
14. G.B. West, D.R. Yennie, Phys. Rev. **172**, 1413 (1968)
15. C.J. Bebek, Phys. Rev. D **17**, 1693 (1978)
16. Review of Particle Physics, Eur. Phys. J. C **15**, 1 (2000)
17. M. Honda et al., Phys. Rev. Lett. **70**, 525 (1993)
18. R.M. Baltrusaitis et al., Phys. Rev. Lett. **52**, 1380 (1984)
19. T.K. Gaisser, U.P. Sukhatme, G.B. Yodh, Phys. Rev. D **36**, 1350 (1987)
20. N.N. Nikolaev, Phys. Rev. D **48**, R1904 (1993)
21. N. Kwak et al., Phys. Lett. B **58**, 233 (1975)
22. U. Amaldi et al., Nucl. Phys. B **166**, 301 (1979)
23. E. Nagy et al., Nucl. Phys. B **150**, 221 (1979)
24. A. Breakstone et al., Phys. Rev. Lett. **54**, 2180 (1985)
25. M. Ambrosio et al., Phys. Lett. B **115**, 495 (1982)
26. A. Breakstone et al., Nucl. Phys. B **248**, 253 (1984)
27. R.E. Breedon et al., Phys. Lett. B **216**, 459 (1989)
28. C. Augier et al., Phys. Lett. B **316**, 448 (1993)
29. F. Abe et al., Phys. Rev. D **50**, 5518 (1993)
30. M. Bozzo et al., Phys. Lett. B **147**, 385 (1984); Phys. Lett. B **155**, 197 (1985)
31. D. Bernard et al., Phys. Lett. B **171**, 142 (1986)
32. BNL-RHIC-PP2PP Experiment, Spokesman W. Guryn, http://www.rhic.bnl.gov/pp2pp/
33. CERN-LHC-TOTEM Experiment, Spokesman G. Matthiae, http:// www.cern.ch/totem/
34. C.W. Akerlof et al., Phys. Rev. D **14**, 2864 (1976)
35. R. Rubinstein et al., Phys. Rev. D **30**, 1413 (1984)
36. R. Cool et al., Phys. Rev. D **24**, 2821 (1981)
37. A. Schiz et al., Phys. Rev. D **24**, 26 (1981)
38. M. Adamus et al., Phys. Lett. B **186**, 223 (1987)
39. D.S. Ayres et al., Phys. Rev. D **15**, 3105 (1976)
40. M. Barth et al., Z. Phys. C **16**, 111 (1982)
41. H. Cheng, J.K. Walker, T.T. Wu, Phys. Rev. D **9**, 747 (1974)